A Space-Time FE Level-set method for convection coupled phase-change processes

L. Boledi[1,*], B. Terschanski[1], S. Elgeti[2,3] and J. Kowalski[1,4]

[1] Aachen Institute for Advanced Study in Computational Engineering Science (AICES), RWTH Aachen University, 52056 Aachen, Germany
email: boledi@aices.rwth-aachen.de, benjamin.terschanski@rwth-aachen.de

[2] Institute of Lightweight Design and Structural Biomechanics (ILSB), TU Wien, 1040 Vienna, Austria
e-mail: elgeti@ilsb.tuwien.ac.at

[3] Chair for Computational Analysis of Technical Systems (CATS), RWTH Aachen University, 52056 Aachen, Germany

[4] Abteilung Computational Geoscience, Georg-August-Universität Göttingen, 37077 Göttingen, Germany
e-mail: julia.kowalski@geo.uni-goettingen.de

Key words: Ghost Cells, Phase Change, Stefan Problem, Space-Time Finite Elements

Abstract: *Phase-transition processes have great relevance for both engineering and scientific applications. In production engineering, for instance, metal welding and alloy solidification are topics of ongoing research, whereas understanding the melting of ice and permafrost is at the centre of many geoscience research questions. In this contribution we focus on one specific phase-change process, namely the convection-coupled solid-liquid phase change of a single species, e.g. water. The material is assumed to be incompressible within the two phases, but we account for density changes across the phase interface. To describe the process, we need to solve the incompressible Navier-Stokes equations and the heat equation for both phases over time. The position of the phase interface is tracked with a level-set method [1]. The level-set function is advected according to the phase interface's propagation speed. Such speed depends on local energy balance across the interface and it is determined through a heat-flux jump condition referred to as the Stefan condition [2]. One of the challenges of this method lies in the approximation of the heat-flux discontinuity at the interface based on the evolving temperature and velocity fields.*

To model the temperature and velocity fields within each phase, we employ the space-time finite element method. However, commonly used interpolation functions, such as piecewise-linear functions, fail to capture discontinuous derivatives over one element that are needed to assess the level-set's transport term. Available solutions to this matter, such as local enrichment with extended finite elements [3], are often not compatible with existing space-time finite element codes and require extensive implementation work. Instead, we consider a different method and we decide to extend the ghost-cell technique to finite element meshes [4]. The idea is that we can separate the two subdomains associated with each phase and solve two independent temperature problems. We prescribe the melting temperature at an additional node close to the interface and we retrieve the required heat flux on each side of the interface. This allows us to locally evaluate the heat-flux jump.

In this work we describe the ghost-cell method applied to our space-time finite element solver [5]. Then, we demonstrate test cases in 3D in view of future applications.

https://doi.org/10.4995/YIC2021.2021.12329

1 INTRODUCTION

In this paper we propose a numerical strategy to simulate convection-coupled solidification and melting processes. Many approaches to track the phase-change interface (PCI) are available [6], but we focus on the level-set method [1]. In our formulation we need to retrieve discontinuities in the first derivatives at the PCI. Extended finite elements solve the problem by locally enriching the basis functions [3], but this changes the number of degrees of freedom over time. Instead, we decide to build upon existing work from Gibou et Al. and extend the ghost-cell approach to our space-time finite element framework [4, 7, 8].

2 NUMERICAL MODELLING

We consider a domain of interest $\Omega \subset \mathbb{R}^d$, where d is the number of space dimensions, that consists of a solid region and a liquid region. The two phases are separated by a distinct PCI. The goal of the model is to determine the evolving velocity, pressure and temperature fields in both phases and over time.

2.1 Governing equations for flow and temperature

Let $t \in (0,T)$ be a time instant. We call $\Omega_1(t)$, $\Omega_2(t)$ the two time-dependent subdomains associated with the liquid region and the solid region, respectively, such that $\Omega_1(t) \cup \Omega_2(t) = \Omega$ for each t. We describe the flow problem with the incompressible Navier-Stokes equations for a Newtonian fluid

$$\rho_* \left(\frac{\partial \mathbf{u}}{\partial t} + \mathbf{u} \cdot \nabla \mathbf{u} - \mathbf{f} \right) + \nabla p - \mu_* \Delta \mathbf{u} = 0 \quad \text{in } \Omega \times (0,T), \tag{1}$$

$$\nabla \cdot \mathbf{u} = 0 \quad \text{in } \Omega \times (0,T), \tag{2}$$

where ρ_* and μ_* denote the density and the dynamic viscosity. To model the temperature field we consider the transient heat equation

$$\rho_* (c_p)_* \left(\frac{\partial T}{\partial t} + \mathbf{u} \cdot \nabla T \right) = \kappa_* \Delta T \quad \text{in } \Omega \times (0,T), \tag{3}$$

where $(c_p)_*$ is the heat capacity and κ_* is the thermal conductivity. The subscript $*$ in Eqs. (1)-(3) indicates the phase-dependent material properties, such that $\rho_*(\mathbf{x},t) = \rho_1$ if $\mathbf{x} \in \Omega_1(t)$ and $\rho_*(\mathbf{x},t) = \rho_2$ if $\mathbf{x} \in \Omega_2(t)$. Note that such properties are phase-wise constant. The advective term $\mathbf{u}$ in Eq. (3) gives rise to a one-way coupling with the Navier-Stokes Equations (1), (2).

We solve both problems with our in-house space-time finite element solver [5, 9]. The stabilised space-time formulation can be found in [10], together with the values for the stabilisation terms.

2.2 Tracking the phase-change interface: Level-set method

We now introduce the level-set formulation to track the evolving PCI. Let $\Phi : \Omega \times (0,T) \to \mathbb{R}$ be a scalar, continuous function such that $\Phi(\mathbf{x},t) < 0$ in $\Omega_1(t)$ and $\Phi(\mathbf{x},t) > 0$ in $\Omega_2(t)$. The phase interface is the zero level set of Φ, that is every $\mathbf{x} \in \Omega : \Phi(\mathbf{x},t) = 0, \forall t \in (0,T)$ [11]. Thus, Φ gives information on which subdomain a point $\mathbf{x}$ is located. We then describe the material properties as function of Φ, e.g. $\rho_* = \rho_1 + (\rho_2 - \rho_1) H_\epsilon(\Phi)$. The function $H_\epsilon(\cdot)$ is the smoothed Heaviside function introduced in [12], which alleviates numerical difficulties.

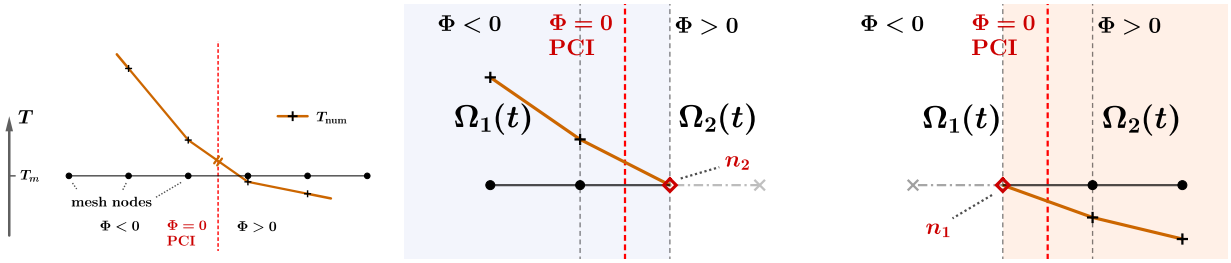

(a) Complete domain (b) Left phase (c) Right phase

Figure 1: 1D example of ghost split. Fig. 1a shows a fictitious temperature field computed on the whole domain. Note that the solution is differentiable across one element and we do not retrieve the heat-flux jump at the PCI. Figs. 1b, 1c show the independent temperature problems solved for each phase after the ghost split. The melting temperature T_m is imposed at the ghost nodes n_1 and n_2.

The evolution of the PCI is described by the level-set equations

$$\begin{aligned} \frac{\partial \Phi}{\partial t} + \mathbf{v} \cdot \nabla \Phi = 0 \quad &\text{in } \Omega \times (0,T), \\ \Phi(\mathbf{x},0) = \Phi_0(\mathbf{x}) \quad &\text{in } \Omega, \end{aligned} \tag{4}$$

where $\mathbf{v}$ denotes the local propagation velocity of the interface. We select the initial condition $\Phi_0(\mathbf{x})$ such that $\Phi(\mathbf{x},t)$ is the signed distance function from the PCI. Problem (4) is a scalar advection problem that shares many similarities with Eq. (3). More details on its space-time formulation are available in Section 3.10 of [13].

Note that the transport term $\mathbf{v}$ in Eq. (4) is not known, so that we need an additional relation to close the problem. Localized at the zero set of the level-set function, the propagation velocity $\mathbf{v}(\mathbf{x},t)$ needs to match the local phase-change rate and can be modelled as the Stefan condition [2]. Thus, $\mathbf{v}$ is proportional to the heat-flux jump at the interface

$$\rho\, h_m \mathbf{v}(\mathbf{x},t) = -\kappa_L \nabla T\big|_{\mathbf{X}^-} + \kappa_S \nabla T\big|_{\mathbf{X}^+} = [\kappa \nabla T]_L^S = q_L - q_S, \quad \forall \mathbf{x} : \Phi(\mathbf{x},t) = 0, \tag{5}$$

where h_m is the latent heat of melting, ρ denotes the material's density, κ the material's conductivity, $\mathbf{X}^{\pm}$ denote the limits taken from either side of the PCI and $[\cdot]_L^S$ refers to the liquid and solid regions. Note that we have closed the problem by coupling the level-set Eq. (4) with the temperature Eq. (3). However, we need to accurately retrieve the discontinuity of the heat flux within our numerical framework, which we will address in the next section.

3 HEAT-FLUX DISCONTINUITY AT THE PHASE INTERFACE

In the previous section we have described our numerical model for melting and solidification problems. What we need is a method to recover the heat-flux jump in Eq. (5) when using finite elements with element-wise continuously differentiable shape functions.

3.1 Evaluation points for the heat fluxes

First, we select evaluation points for the representative fluxes q_L, q_S in Eq. (5). The intuitive approach would be to choose points normal to the PCI, but this presents issues since the normal is not well-defined at the intersections with the mesh. Thus we adopt a different approach based on three assertions:

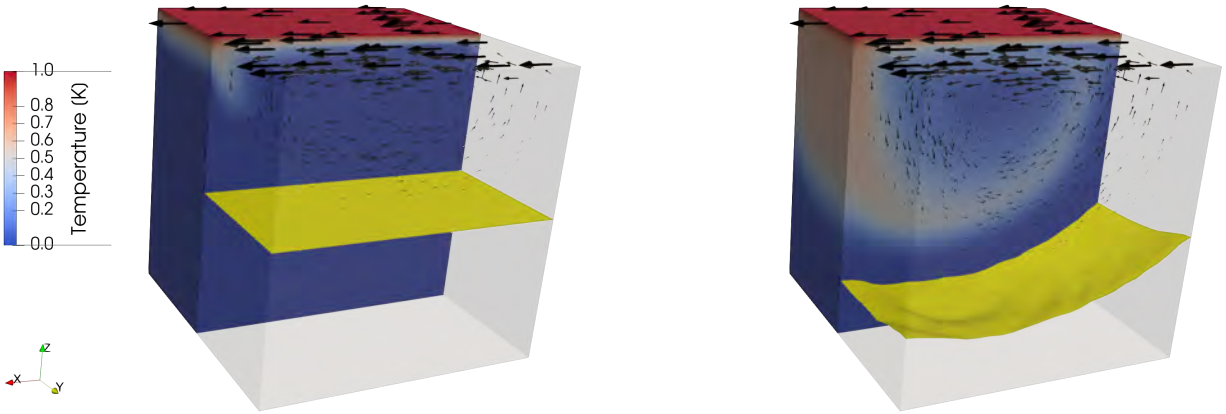

(a) $t = 1s$ (b) $t = 15s$

Figure 2: Phase-change coupled 3D lid-driven cavity. The temperature profile is shown at two different time instants. The yellow surface denotes the phase-change interface. The black arrows represent the velocity vectors at each point, their size is proportional to the velocity magnitude. The domain is transparent for $y > 0.5$.

1. If an element face is cut by the PCI, we consider the nodes that belong to the face as flux nodes. We use the numerical gradients at these nodes as representative fluxes in Eq. (5). The sign of the level-set function carries information on the corresponding phase q_L or q_S;

2. Each nodal gradient is computed as the arithmetic average of the gradients on all the elements that surround the node;

3. If the PCI intersects a mesh node, we consider the average of all the nodes in the adjacent faces.

3.2 The ghost-split method

The second issue comes from the computation of the numerical gradient, since its mathematical properties depend on the properties of the basis functions. In particular, we employ piecewise linear shape functions that can show discontinuities in the heat flux only at element nodes. This is where the ghost split comes into play. Since we know that the temperature solution at the PCI must equal the melting temperature T_m at each time instant, the PCI can be viewed as a Dirichlet type boundary for each phase. Then, we solve two independent temperature problems in each subdomain and retrieve the representative fluxes to compute the interface propagation velocity as in Eq. (5). However boundary conditions can be imposed only on mesh nodes, so we have to consider additional nodes for each subdomain to enforce the melting temperature at the approximate position of the PCI. These extra nodes are called ghost nodes. Figure 1 shows an example of ghost split for a 1D temperature profile. By solving two separate problems on each subdomain, we can retrieve the heat-flux jump at the PCI.

Now we can compute the interface velocity at the intersections with the mesh. As a last step we need to define the transport term $\mathbf{v}$ of Eq. (4) on all the mesh nodes. Given the Stefan velocity computed on a crossing, we extend such velocity to all the nodes that are closest to the crossing. Note that we do not need an additional search to find the nearest neighbours of

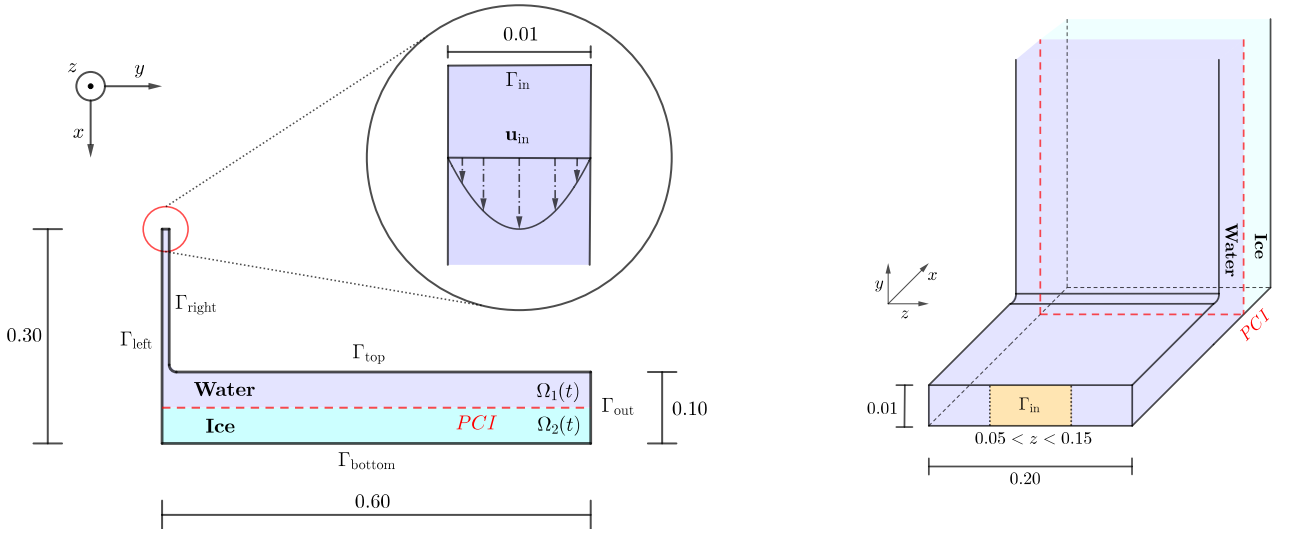

(a) Top view of the domain

(b) Close-up of the inflow

Figure 3: Phase-change coupled 3D corner flow. We show the computational domain of the second test case (not drawn to scale). On the left, a top view section is displayed. On the right, we show a close-up of the inflow to call attention to the boundary condition. Note that the parabolic velocity profile is imposed only on the part highlighted in orange.

the mesh nodes, as reinitialising the level-set function entails this information.

Recall that with the ghost split the melting temperature is assigned at an additional node close to the PCI. By doing so, we introduce an error in the interface location computed at the subsequent time step. Note, however, that the error depends on the mesh resolution and the position of the ghost node converges to the correct location of the PCI for finer grids [4]. Higher order schemes for the temperature extrapolation are available and can be investigated in the future [7].

4 NUMERICAL EXAMPLES

In the last section we show two different numerical cases in 3D. A detailed verification of the numerical method against the one-phase Stefan problem can be found in [14], together with additional 2D examples. In this work we focus only on tridimensional problems in view of more complex applications.

Recall that the presented numerical method is not bound to the number of spatial dimensions. We have described the 1D ghost split in Fig. 1 for the sake of clarity, but a more detailed graphical description on a 2D mesh is available in [14]. Thus, the space-time finite element solver can handle 3D phase-change processes. Performance issues might arise with very fine meshes, for instance in the reinitialisation of the level-set function. However different strategies are available, e.g. the fast marching method [15], that can be investigated in the future.

4.1 Phase-change coupled 3D lid-driven cavity

We consider a $1 \times 1 \times 1$ domain, i.e. a unit cube, which is initially solid for $z < 0.5$ and liquid for $z > 0.5$. At the lateral and bottom boundaries we impose homogeneous Dirichlet boundary conditions for the velocity and homogeneous Neumann conditions for temperature. At the top edge we impose the temperature $T = 1$ and the velocity in x direction $\mathbf{u} = [1, 0, 0]^\intercal$. The initial temperature is $T_m = 0$. We select the parameters for the two phases ρ_1 =2, ρ_2 =1,

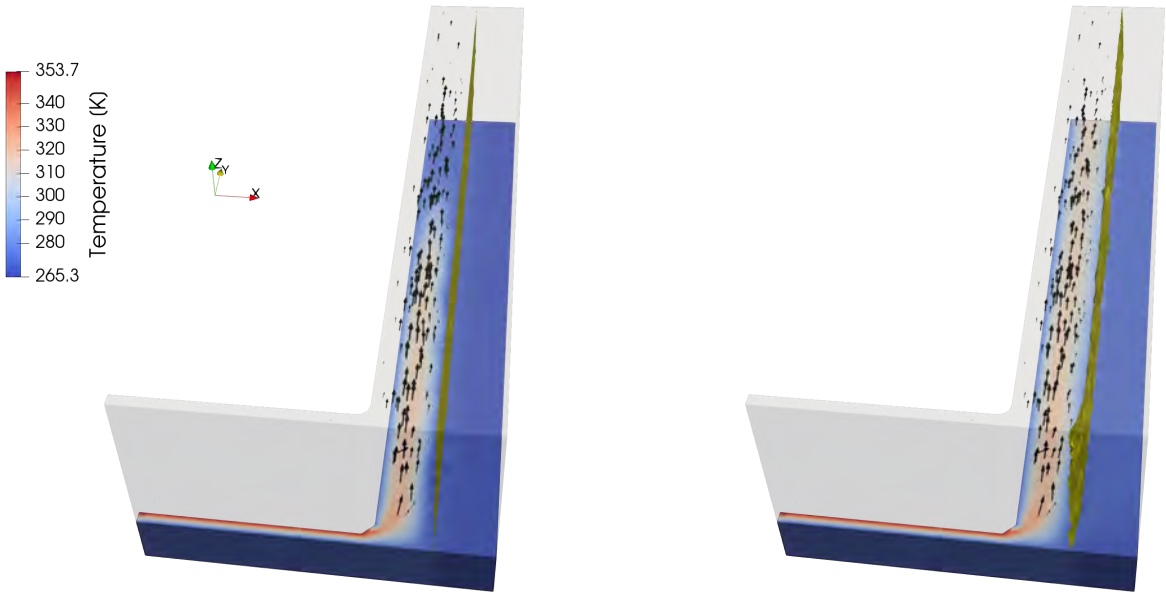

(a) $t = 50s$ (b) $t = 2500s$

Figure 4: Phase-change coupled 3D corner flow. The temperature profile is shown at two different time instants. The yellow surface denotes the phase-change interface. The black arrows represent the velocity vectors at each point, their size is proportional to the second component of velocity. The domain is transparent for $z > 0.05$.

$(c_p)_1$ =1e3, $(c_p)_2$ =1, κ_1 =1, κ_2 =1, μ_1=1, μ_2=1e4 and h_m =1, where all the values are in SI units. We simulate 500 time steps with $\Delta t = 0.1s$ on a uniform structured grid that comprises 35152 nodes.

Figure 2 shows the computed temperature profile at two time instants. After 10 time steps the PCI has not moved yet, but we retrieve the expected anti-clockwise circulation in the liquid region (2a). After 150 time steps the PCI has moved downwards (2b). Note that the left side of the domain melts faster, since the temperature propagation is driven by the convection of the flow field.

4.2 Phase-change coupled 3D corner flow

For the second example we consider a recent research topic, namely the flow that develops around a thermal melting cryorobot that descents into the ice [16]. Figure 3 shows the geometry of the test case, which resembles an idealised probe moving to the right. The inflow channel turns 90 degrees into a wider outflow channel. The latter contains two different phases that are separated by an evolving PCI. We impose a parabolic velocity profile at the inflow such that $\mathbf{u}_{\text{in}} = [5000y\,(0.01 - y), 0, 0]^\intercal$ if $0.05 < z < 0.15$. Furthermore, we impose no-slip conditions at each boundary except for the inflow and the outflow. We have Dirichlet temperature conditions on Γ_{right} and Γ_{top}, $T = 353\,\text{K}$ and $T = 278\,\text{K}$ respectively. On Γ_{left} we prescribe $T = 273\,\text{K}$ if $x < 0.25$, $T = 268\,\text{K}$ if $x > 0.25$. The initial conditions are $\mathbf{u}(\mathbf{x}, 0) = \mathbf{0}$, $T(\mathbf{x}, 0) = 273\,\text{K}$ in $\Omega_{1,0}$, $T(\mathbf{x}, 0) = 268\,\text{K}$ in $\Omega_{2,0}$. The material properties are selected according to water ice [17]. We simulate 500 time steps with $\Delta t = 5s$.

Figure 4 shows the computed temperature profile at two time instants. At the final time step a bulge is visible in the PCI. As expected, the ice melts as we introduce heat into the system and we can see the effect right after the 90 degree turn. We recall that this setup is not reproducible in 2D as heat and flow are applied only on a portion of the inflow, which

underlines the need for a numerical method that can represent 3D physical phenomena.

ACKNOWLEDGEMENTS

The authors were supported by the Helmholtz Graduate School for Data Science in Life, Earth and Energy (HDS-LEE). The work was furthermore supported by the Federal Ministry of Economic Affairs and Energy, on the basis of a decision by the German Bundestag (50 NA 1908). The authors gratefully acknowledge the computing time granted by the JARA Vergabegremium and provided on the JARA Partition part of the supercomputer JURECA at Forschungszentrum Jülich [18].

REFERENCES

[1] S. Osher and J. A. Sethian. Fronts propagating with curvature-dependent speed: Algorithms based on Hamilton-Jacobi formulations. *Journal of Computational Physics*, 79(1):12 – 49, 1988.

[2] S. Chen, B. Merriman, S. Osher, and P. Smereka. A Simple Level Set Method for Solving Stefan Problems. *Journal of Computational Physics*, 135(1):8 – 29, 1997.

[3] M. Bernauer and R. Herzog. Motion Planning for the Two-Phase Stefan Problem in Level Set Formulation 1, 12 2010.

[4] F. Gibou, R. Fedkiw, L.-T. Cheng, and M. Kang. A Second-Order-Accurate Symmetric Discretization of the Poisson Equation on Irregular Domains. *Journal of Computational Physics*, 176:205–227, 02 2002.

[5] T. E. Tezduyar, M. Behr, S. Mittal, and A. A. Johnson. Computation of unsteady incompressible flows with the stabilized finite element methods: Space-time formulations, iterative strategies and massively parallel implementations. In *New Methods in Transient Analysis*, American Society of Mechanical Engineers, Pressure Vessels and Piping Division (Publication) PVP, pages 7–24. ASME, December 1992. Winter Annual Meeting of the American Society of Mechanical Engineers.

[6] S. Elgeti and H. Sauerland. Deforming fluid domains within the finite element method: Five mesh-based tracking methods in comparison. *Archives of Computational Methods in Engineering*, 23:323–361, 2016.

[7] F. Gibou and R. Fedkiw. A fourth order accurate discretization for the Laplace and heat equations on arbitrary domains, with applications to the Stefan problem. *Journal of Computational Physics*, 202:577–601, 01 2005.

[8] F. Gibou, L. Chen, D. Nguyen, and S. Banerjee. A level set based sharp interface method for the multiphase incompressible navier–stokes equations with phase change. *Journal of Computational Physics*, 222:536–555, 03 2007.

[9] T. E. Tezduyar, M. Behr, S. Mittal, and J. Liou. A new strategy for finite element computations involving moving boundaries and interfaces—the deforming-spatial-domain/space-time procedure: II. computation of free-surface flows, two-liquid flows, and flows with drifting cylinders. *Computer Methods in Applied Mechanics and Engineering*, 94(3):353–371, 1992.

[10] L. H. Pauli, S. T. Haßler, and M. Behr. Stabilized Finite Element Methods for Computational Design of Blood-Handling Devices. In *International Workshop on Modelling and Simulation in Biomedical Applications, 2017-10-24 - 2017-10-25, Mariatrost, Austria*, Oct 2017.

[11] A. Quarteroni. *Numerical Models for Differential Problems*. MS&A. Springer Milan, 2010.

[12] J. A. Sethian and P. Smereka. Level set methods for fluid interfaces. *Annual Review of Fluid Mechanics*, 35(1):341–372, 2003.

[13] J. Donea and A. Huerta. *Finite Element Methods for Flow Problems*, chapter 3, pages 79–146. John Wiley & Sons, Ltd, 2005.

[14] L. Boledi, B. Terschanski, S. Elgeti, and J. Kowalski. A level-set based space-time finite element approach to the modelling of solidification and melting processes. *Manuscript submitted for publication*, 2021. Preprint available at https://arxiv.org/abs/2105.09286.

[15] R. Kimmel and J. A. Sethian. Computing geodesic paths on manifolds. *Proceedings of the National Academy of Sciences of the United States of America*, 95(15):8431—8435, July 1998.

[16] B. Dachwald, J. Mikucki, S. Tulaczyk, I. Digel, C. Espe, M. Feldmann, G. Francke, J. Kowalski, and C. Xu. Icemole: a maneuverable probe for clean in situ analysis and sampling of subsurface ice and subglacial aquatic ecosystems. *Annals of Glaciology*, 55(65):14–22, 2014.

[17] S. Ulamec, J. Biele, O. Funke, and M. Engelhardt. Access to glacial and subglacial environments in the Solar System by melting probe technology. *Environmental Science and Bio/Technology*, 6:71–94, 01 2007.

[18] Jülich Supercomputing Centre. JURECA: Modular supercomputer at Jülich Supercomputing Centre. *Journal of large-scale research facilities*, 4(A132), 2018.